

Article

Fabrication of Electrochemical Sensor for the Detection of Mg(II) Ions Using CeO₂ Microcuboids as an Efficient Electrocatalyst

Girdega Muruganandam ¹, Noel Nesakumar ^{1,2}, Arockia Jayalatha Kulandaisamy ³, John Bosco Balaguru Rayappan ^{2,3,*} and Balu Mahendran Gunasekaran ⁴ 

¹ School of Chemical & Biotechnology (SCBT), SASTRA Deemed University, Thanjavur 613401, Tamil Nadu, India; 125078008@sastra.ac.in (G.M.); noel@scbt.sastra.edu (N.N.)

² Centre for Nanotechnology & Advanced Biomaterials (CeNTAB), SASTRA Deemed University, Thanjavur 613401, Tamil Nadu, India

³ School of Electrical & Electronics Engineering (SEEE), SASTRA Deemed University, Thanjavur 613401, Tamil Nadu, India; arockiajayalatha@eee.sastra.edu

⁴ Department of Chemistry, A.V.V.M Sri Pushpam College (Autonomous), Bharathidasan University, Poondi 613503, Tamil Nadu, India; mahibalu2010@gmail.com

* Correspondence: rjbosco@ece.sastra.edu; Tel.: +91-4362-264-101 (ext. 255); Fax: +91-4362-264-120

Abstract: In human blood serum, the concentration of magnesium ions typically ranges from 0.7 mM to 1.05 mM. However, exceeding the upper limit of 1.05 mM can lead to the condition known as hypermagnesemia. In this regard, a highly sensitive and selective electrochemical sensor for Mg(II) ion detection was successfully fabricated by immobilizing cerium oxide (CeO₂) microcuboids, synthesized via microwave radiation method, onto the surface of glassy carbon electrode (GCE). Cyclic voltammetry studies revealed the exceptional electrocatalytic effect of CeO₂ microcuboid-modified GC electrode, particularly in relation to the irreversible reduction signal of Mg(II). The microcuboid-like structure of CeO₂ microparticles facilitated enhanced adsorption of Mg(II) ion ($\Gamma = 2.17 \times 10^{-7} \text{ mol cm}^{-2}$) and electron transfer ($k_s = 8.94 \text{ s}^{-1}$) between the adsorbed Mg(II) ions and GCE. A comprehensive analysis comparing the performance characteristics of amperometry, differential pulse voltammetry, cyclic voltammetry, and square wave voltammetry was conducted. The square wave voltammetry-based Mg(II) sensor exhibited remarkable sensitivity of 2.856 $\mu\text{A mM}^{-1}$, encompassing a broad linear detection range of 0–3 mM. The detection and quantification limits were impressively low, with values of 19.84 and 66.06 μM , respectively. Remarkably, the developed electrode showed a rapid response time of less than 140 s. Multiple linear regression and partial least squares regression models were employed to establish a mathematical relationship between magnesium ion levels and electrochemical parameters. Notably, the proposed sensor exhibited excellent anti-interferent ability, repeatability, stability, and reproducibility, enabling the fabricated electrode to be used effectively for Mg(II) ion sensing in real-world samples.

Keywords: Mg(II) ion sensor; CeO₂ microcuboids; glassy carbon electrode; voltammetry; electrochemical parameters



Citation: Muruganandam, G.; Nesakumar, N.; Kulandaisamy, A.J.; Rayappan, J.B.B.; Gunasekaran, B.M. Fabrication of Electrochemical Sensor for the Detection of Mg(II) Ions Using CeO₂ Microcuboids as an Efficient Electrocatalyst. *Chemosensors* **2023**, *11*, 442. <https://doi.org/10.3390/chemosensors11080442>

Academic Editors: Andrey Bratov and Danila Moscone

Received: 25 June 2023

Revised: 17 July 2023

Accepted: 4 August 2023

Published: 7 August 2023



Copyright: © 2023 by the authors. Licensee MDPI, Basel, Switzerland. This article is an open access article distributed under the terms and conditions of the Creative Commons Attribution (CC BY) license (<https://creativecommons.org/licenses/by/4.0/>).

1. Introduction

Magnesium is an indispensable element that is crucial for a vast array of physiological processes [1]. Specifically, it plays a pivotal role in regulating essential processes such as vitamin D and calcium levels, neurotransmitter release, nerve conduction, muscle relaxation and contraction, adenosine triphosphate production, DNA and protein synthesis, immune system function, and genetic material integrity in cells [2]. Moreover, it aids in maintaining a healthy heart rhythm and blood pressure, which are critical for overall health. In human blood serum, magnesium ions are typically present in concentrations ranging

from 0.7 mM to 1.05 mM [3]. However, exceeding the upper limit of 1.05 mM can result in hypermagnesemia, a condition that can lead to serious complications, such as respiratory depression, low blood pressure, cardiac arrest, vomiting, nausea, lethargy, weakness, impaired kidney function, and myasthenia gravis [4]. Given the paramount importance of maintaining optimal magnesium levels in the body and the potential risks associated with hypermagnesemia, there is a pressing need to develop highly sensitive and selective sensors for the detection of magnesium ions [5–9]. In the realm of detecting magnesium ions in human blood serum, a diverse range of analytical methods are employed, including enzymatic assays, colorimetric assays, inductively coupled plasma mass spectrometry, and atomic absorption spectroscopy [5–9]. Despite the general perception of these methods as specific, sensitive, and reliable, each one has inherent limitations. The presence of inhibitors and activators in the sample affects the selectivity and sensitivity of enzyme and colorimetric assays [10]. In contrast, inductively coupled plasma mass spectrometry and atomic absorption spectroscopy require additional equipment and skilled personnel for sample preparation, which can be both time-consuming and expensive [10]. As an attractive alternative, electrochemical sensors offer a multitude of advantages [11]. They are affordable, highly sensitive, portable, and boast a rapid response time.

Electroanalytical techniques have been extensively employed to detect magnesium ions, including differential pulse voltammetry, potentiometry, and electrochemical impedance spectroscopy [5–9]. However, the sensitivity of these methods for detecting changes in magnesium ion concentration has not been compared in previous studies, creating a critical gap in the field [5–9]. In light of this, this study seeks to address this gap by comparing the electroanalytical performance characteristics of cyclic voltammetry, square wave voltammetry, differential pulse voltammetry, and amperometry for detecting changes in magnesium ion concentration. The development of electrochemical sensors for magnesium ion detection can be achieved by modifying the surface of the glassy carbon electrode (GCE) with efficient nanomaterials. Nanomaterials, including multi-walled carbon nanotubes, ionophores, zinc oxide nanorods, magnesium ferrite nanoparticles, magnesiochromite nanoparticles, and nickel disulfide nanoparticles, have been extensively used to improve the performance of electrochemical sensors for magnesium ion detection [5–9]. These materials possess unique properties that enable them to modify the electrode surface on a nanoscale level, resulting in swift electrode kinetics, high electroactive area, enhanced conductivity, and increased catalytic activity.

To the best of our knowledge, no reports on the fabrication of electrochemical sensors for the detection of Mg^{2+} ions using cerium oxide (CeO_2) nanoparticles as an efficient sensing platform are available. Nevertheless, within the past decade, the distinctive properties of CeO_2 nanoparticles, including increased electroactive surface area, high ionic conductivity, mechanical stability, thermal stability, and biocompatibility, have garnered substantial attention in the field of electrochemical sensor development [12–16]. Consequently, CeO_2 nanoparticles are an auspicious material for use as an efficient biosensing platform, particularly for detecting metal ions at ultralow concentrations [12–16]. One of the prominent features of CeO_2 nanoparticles is their ability to exist in both 3+ and 4+ states, which allows for reversible transition between Ce(III) and Ce(IV) oxidation states [17–19]. These attributes have stimulated considerable interest among researchers as a promising nanoparticle for the development of electrochemical sensors.

This work involved the synthesis of CeO_2 nanoparticles using the microwave radiation method, which were then employed as a nanointerface to modify the surface of GCE using chitosan as an outer membrane in order to develop GC/ CeO_2 electrode. Later, the electrocatalytic properties of CeO_2 nanoparticles towards the oxidation and reduction of magnesium ions were studied using cyclic voltammetry as an electroanalytical technique. Subsequently, the analytical performance of the GC/ CeO_2 electrode in detecting varying levels of magnesium ions was evaluated using cyclic voltammetry, square wave voltammetry, differential pulse voltammetry, and amperometry, with the results compared to assess the effectiveness of each technique. Finally, calibration equations were formu-

lated using multiple linear regression and partial least squares regression methods based on electrochemical parameters derived from square wave voltammograms for different concentrations of magnesium ions.

2. Experimental

2.1. Materials and Reagents

Cerium nitrate, dopamine, magnesium chloride, L-cysteine, sodium citrate, calcium, glucose, sodium hydroxide, ethanol, lactic acid, urea, uric acid, creatinine, ascorbic acid, trisodium phosphate, alumina, potassium chloride, and trisodium phosphate were procured from Merck India Ltd., India. All aqueous solutions were prepared using deionized water obtained from the Milli-Q system. The employed reagents were of analytical quality and are utilized as received.

2.2. Synthesis of CeO₂ Microcuboids

The synthesis of cerium oxide microcuboids involved the utilization of microwave radiation (Multiwave 3000 microwave sample system, Anton Paar, Synthos; Power: 800 W). To commence the process, a solution comprising 0.2 mM of cerium nitrate and 0.1 mM of sodium citrate in 150 mL of deionized water was prepared. The resulting solution was then subjected to vortex mixing at 1200 rpm for 30 min in an ice bath, followed by a 10-min rest period at room temperature. Subsequently, the solution was transferred to a Teflon vessel capable of withstanding microwave heating and exposed to microwave radiation for 1 h at 200 °C, which resulted in the appearance of a yellow precipitate. Following the microwave irradiation treatment, the product was allowed to cool to room temperature for 45 min, after which it underwent centrifugation at 3000 rpm for 20 min to eliminate excess sodium hydroxide. This centrifugation process was repeated several times, with each cycle consisting of the removal of the supernatant, resuspension of the precipitate, and centrifugation with ethanol and deionized water four times each. Later, the rinsed precipitates were dried overnight at 60 °C in a hot-air oven to ensure complete drying. Finally, the dried precipitates were carefully crushed to a fine powder using a mortar and pestle.

2.3. Fabrication of CeO₂ Microcuboid-Modified GCE

To fabricate the CeO₂ microcuboid-modified GCE, the initial step involved polishing the surface of the GCE with 3 mm-diameter alumina powder, followed by sonicating the electrode for 2 min with a solution of distilled water and ethanol, until a mirror-like shiny surface was obtained. Subsequently, 1 mg of as-synthesized CeO₂ microcuboids was dispersed in 0.1 mL of ethanol solution and sonicated for 30 min until complete dispersion was attained. Then, 3 µL of the dispersed mixture was drop-casted onto the pre-cleaned GCE surface and left to dry naturally at room temperature for 12 h, resulting in the development of CeO₂/GCE. Finally, the fabricated electrode was placed in a refrigerator at 0 °C in the refrigerator for storage prior to further electrochemical analysis.

2.4. Material Characterization

The attenuated total reflectance–Fourier-transform infrared (ATR-FTIR) spectrum of the as-synthesized CeO₂ microcuboids was recorded using Alpha T FT-IR spectrometer from Bruker, Germany over a spectral range of 4000–400 cm⁻¹ to study the presence of functional groups on as-synthesized CeO₂ powder sample. In addition, field-emission scanning electron microscopy (FE-SEM) was performed using JSM6701F, JEOL, Japan, to record the morphological images of the as-synthesized CeO₂ powder sample. An X-ray diffractometer (XRD), Rigaku Ultima III, USA was employed to characterize the crystal structure of as-synthesized CeO₂ microcuboids. X-ray photoelectron spectroscopy (ThermoFisher scientific, Loughborough, UK) was utilized to investigate the chemical composition of the CeO₂ microcuboids. Electrochemical measurements were performed using an electrochemical workstation (CHI600E, Sinsil International Pvt Ltd, Bangalore,

India) in order to conduct cyclic voltammetry, differential pulse voltammetry, square wave voltammetry, and amperometry analysis. The fabricated CeO_2/GCE served as the working electrode for magnesium ion sensing, while Ag/AgCl saturated in KCl and Pt wire served as the reference and counter electrodes, respectively (Figure 1). Cyclic voltammetry measurements were conducted in the applied potential range of -0.13 to 0.72 V at a scan rate of 0.1 Vs^{-1} in 0.1 M KCl at $\text{pH } 7.0$. Amperometry measurements were performed at an applied potential of 0.393 V (vs. Ag/AgCl). Square wave and differential pulse voltammetric measurements were performed in the potential range of -0.13 to 0.72 V by immersing CeO_2/GCE in 0.1 M KCl ($\text{pH } 7.0$) solution. The following operational settings were used for differential pulse voltammetry: an increment potential of 4 mV, a final potential of 0.72 V, an initial potential of -0.13 V, a pulse width of 0.06 s, an amplitude of 50 mV, a pulse period of 0.5 s, and a sampling width of 0.02 s. For square wave voltammetry, the settings were as follows: an initial potential of -0.13 V, a final potential of 0.72 V, an increment potential of 4 mV, an amplitude of 25 mV, and a frequency of 15 Hz. All electrochemical measurements were carried out at room temperature in the concentration range of 0 – 3 mM to obtain the calibration curve of the CeO_2 modified GCE.

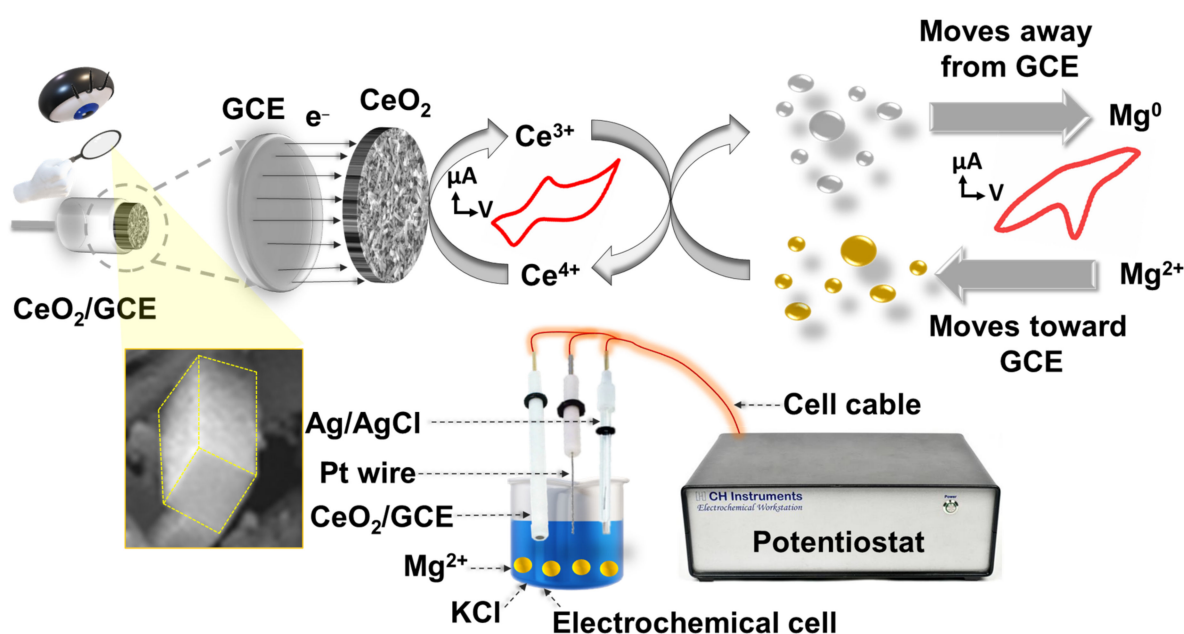


Figure 1. Schematic illustration of electrochemical measurement for the detection of magnesium ions using CeO_2 -modified GCE.

2.5. Partial Least Squares Regression and Multiple Linear Regression Analysis

The most common method for estimating the relationship between independent and dependent variables is the regression model. The prognostication of magnesium ion concentration in 0.1 M KCl solution ($\text{pH } 7.0$) is accomplished by exploiting variations in one or more electrochemical parameters, specifically by employing multiple linear regression and partial least squares regression models [20]. The utilization of multiple linear regression and partial least squares regression models serves the purpose of (i) establishing a correlation between the concentration of magnesium ions and various electrochemical parameters, namely, surface coverage, peak area, peak current, maximum ascending slope, and minimum descending slope, and the concentration of magnesium ions, and (ii) estimating the concentration of magnesium ions by considering the variations in the electrochemical parameters. Multiple linear regression analyzes the linear association between the concentration of magnesium ions and multiple electrochemical parameters, while partial least squares regression extracts latent variables from both the concentration of magnesium ions and multiple electrochemical parameters to establish a linear regression model [20]. The

model equations representing partial least squares regression and multiple linear regression are expressed as:

$$[Mg^{2+}] = a_0 + a_1[peak\ area] + a_2[\Gamma] + a_3[maximum\ slope] + a_4[minimum\ slope] + a_4[I_p] \quad (1)$$

where a_0 represents the intercept, $[Mg^{2+}]$ denotes the magnesium ion concentration in millimolar (mM), *peak area* is the area beneath the peak current measured in amperes per volt (AV), I_p denotes the cathodic peak current measured in microamperes (μA), *maximum slope* corresponds to the highest value of the ascending slope, *minimum slope* corresponds to the lowest value of the descending slope, Γ represents the surface coverage measured in picomoles per square centimeter ($pM\ cm^{-2}$) and a_1 , a_2 , a_3 , and a_4 refer to the coefficients associated with the independent variables *peak area*, Γ , *maximum slope*, *minimum slope* and I_p , respectively. An estimation of the coefficients of the multiple linear regression and partial least squares regression models allows the concentration of magnesium ions to be predicted based on the values of the electrochemical parameters. Through the estimation of these coefficients within both the multiple linear regression and partial least squares regression models, it becomes possible to predict the concentration of magnesium ions based on the respective values of the electrochemical parameters. Both the statistical methodologies of partial least squares regression and multiple linear regression were executed through the utilization of the MATLAB 2022b software package.

3. Results and Discussion

3.1. Characterization of CeO₂ Microcuboids

Figure 2a illustrates the FE-SEM image portraying the as-synthesized CeO₂ powder sample. The FE-SEM image discloses the cuboid-shaped morphology of the CeO₂ microparticles, with dimensions of 167 nm in width, 163 nm in height, and 976 nm in length. Moreover, the FE-SEM image showcases the uniform dispersion of the CeO₂ microcuboids on the GCE surface, exhibiting a homogeneous particle distribution with a relative standard deviation (RSD) of less than 5.12%.

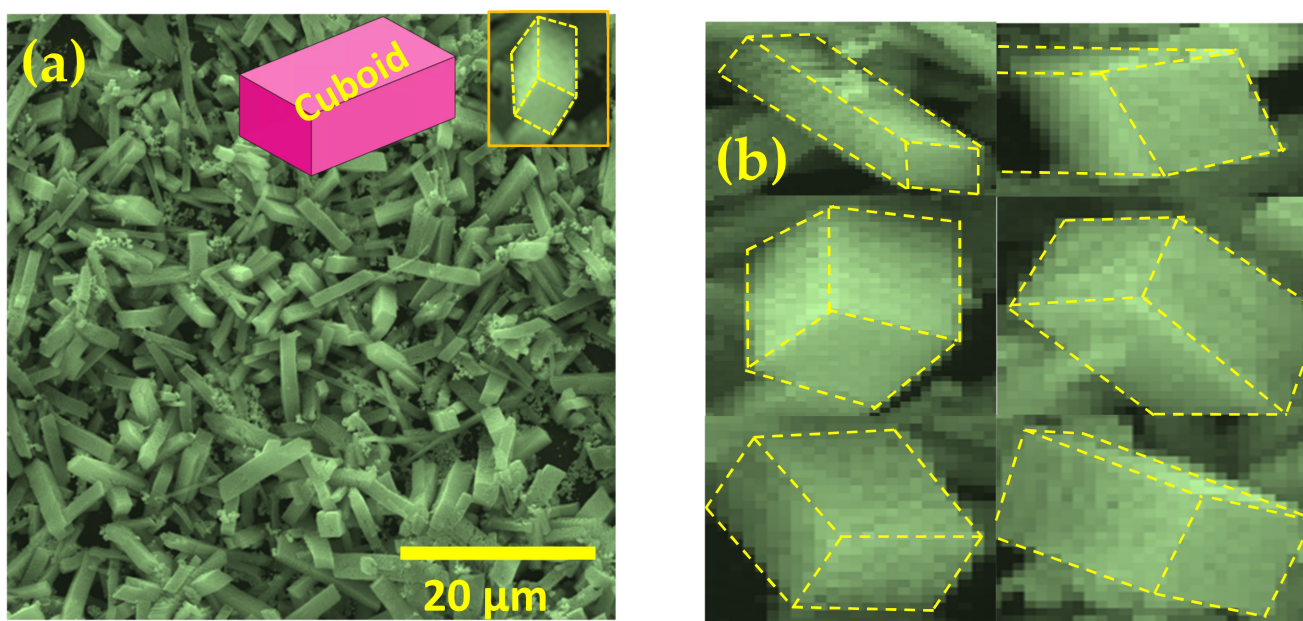


Figure 2. Cont.

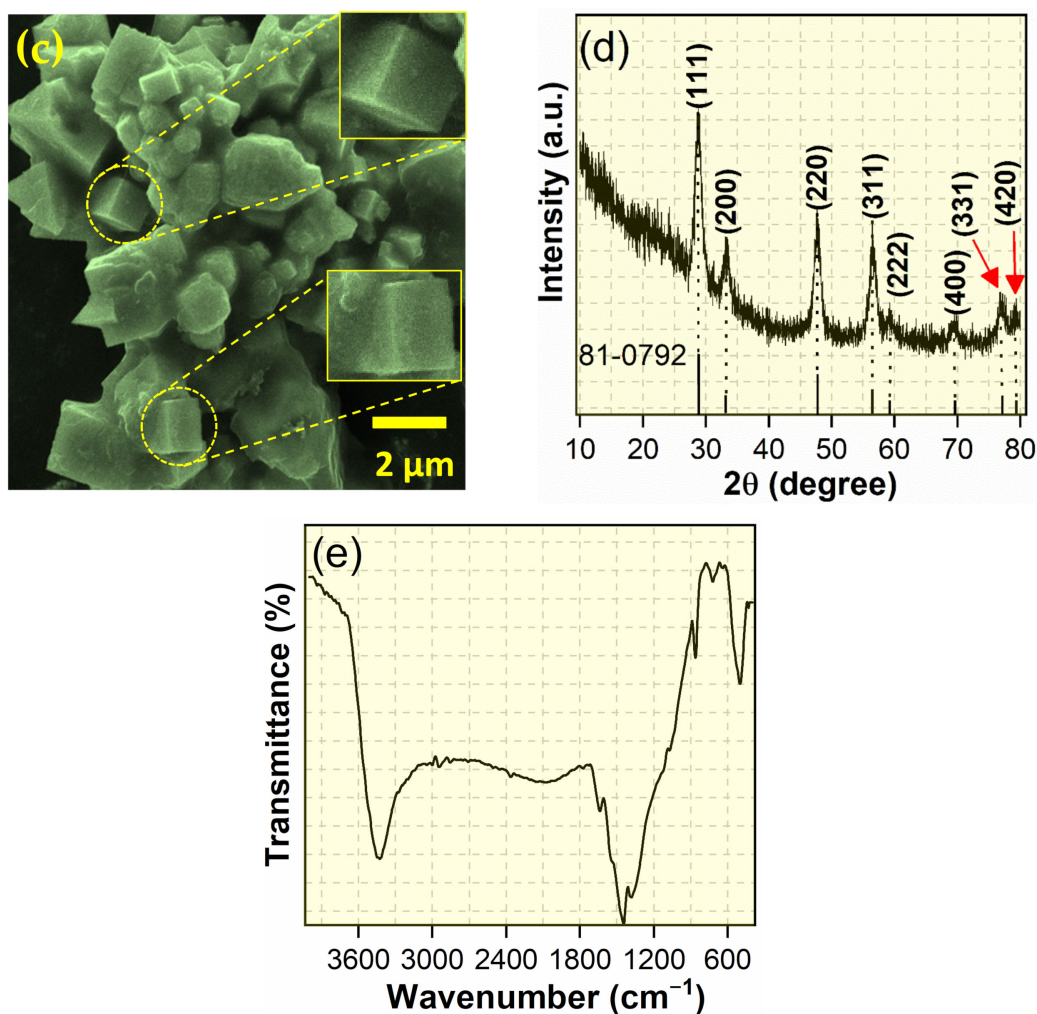


Figure 2. (a–c) Field-emission scanning electron microscopy images, (d) X-ray diffraction pattern, and (e) Fourier-transform infrared spectrum of CeO₂ microcuboids.

Figure 2b exhibits the XRD pattern of the synthesized CeO₂ microcuboids. The XRD pattern reveals the presence of eight broad peaks located at 2θ angles of 28.72° , 33.23° , 47.54° , 56.40° , 59.17° , 69.45° , 76.96° , and 79.33° , corresponding to the (111), (200), (220), (311), (222), (400), (331), and (420) crystallographic planes, respectively. This XRD pattern confirms the cubic structure of the synthesized CeO₂ microparticles. Furthermore, the observed XRD peaks are consistent with the findings reported by Sayyed et al. [21] and match precisely with JCPDS card no. 81-0792. Importantly, the absence of diffraction peaks attributable to impurities, such as Ce(OH)₂, is evident in the XRD pattern. The mean crystallite size of the CeO₂ powder sample was estimated through the application of the Debye-Scherrer formula, yielding a value of 16.2 nm.

Figure 2c illustrates the FTIR spectrum obtained for CeO₂ microcuboids. The spectrum reveals discernible bands at specific wavenumbers, namely, 3437, 1646, 1541, 1440, 1380, 1068, 858, 717, and 498 cm⁻¹. Notably, a pronounced peak at 1440 cm⁻¹ corresponds to the bending vibration associated with C-H stretching [22–24]. The presence of molecular water is manifested by the characteristic peak located at 1646 cm⁻¹, which can be ascribed to the bending vibration and interlayer stretching phenomena [22–24]. The transmittance peak observed at 3437 cm⁻¹ provides compelling evidence for the presence of OH groups on the surface of CeO₂ microcuboids, attributable to their interaction with water during the preparation stage [22–24]. The transmittance peak at 1380 cm⁻¹ is attributed to the stretching vibration of N-O due to the presence of nitrate within the precursor [22–24]. Similarly, the band at 1541 cm⁻¹ characterizes the anti-symmetric stretching of COO- groups,

while the transmittance band detected at 1068 cm^{-1} signifies the C-OH stretch [22–24]. The well-defined, sharp transmittance bands centered at 858 cm^{-1} , accompanied by the band positioned at 717 cm^{-1} , correspond to the envelope of the phonon band exhibited by CeO_2 microcuboids [22–25]. The transmittance peak recorded at 498 cm^{-1} confirms the $\nu(\text{O}-\text{Ce}-\text{O})$ vibration, thereby corroborating the formation of CeO_2 microcuboids [22–24]. Taken together, these results provide confirmation that the powder sample was CeO_2 .

XPS was employed to investigate the elemental composition and chemical states of CeO_2 microcuboids. The high-resolution XPS survey scan of CeO_2 is shown in Figure 3a. The XPS survey scan spectrum indicated that CeO_2 microcuboids comprise Ce 3d, O 1s, and C 1s. Figure 3b shows the XPS Ce 3d spectrum. As can be seen from Figure 3b, eight discernible peaks were identified in the high-resolution XPS Ce 3d spectrum, which can be ascribed to the spin-orbit splitting in Ce $3d_{3/2}$ and Ce $3d_{5/2}$ [26–28]. This splitting phenomenon suggests the coexistence of Ce^{4+} and Ce^{3+} oxidation states within the CeO_2 microcuboids [26–28]. Detailed analysis of the data reveals that the peaks at binding energies of 898.02, 902.95, 909.89, and 918.34 eV can be assigned to the ionization of Ce $3d_{3/2}$, whereas the peaks at binding energies of 879.49, 883.28, 887.71, and 895.15 eV correspond to the ionization of Ce $3d_{5/2}$ [26–28]. Notably, the decomposition peaks observed at binding energy values of 879.49, 887.71, 895.15, 898.02, 909.89, and 918.34 eV unequivocally indicate the presence of Ce^{4+} 3d states, thereby confirming the valence state of Ce in the sample as +4 [26–28]. Conversely, the decomposition peaks detected at binding energies of 883.28 and 902.95 eV are attributed to the valence state of Ce^{3+} [26–28]. The high-resolution XPS O 1s spectrum is shown in Figure 3c. The peak exhibiting high intensity at a binding energy of 528.48 eV corresponds to the lattice oxygen within the CeO_2 microcuboids [26–28]. Conversely, the two remaining XPS decomposition peaks observed at binding energies of 530.67 and 532.76 eV may arise from the oxygen deficiency region within the CeO_2 matrix, or the presence of water, hydroxyl groups, or loosely bound adsorbed oxygen within the vacant lattice sites [26–28].

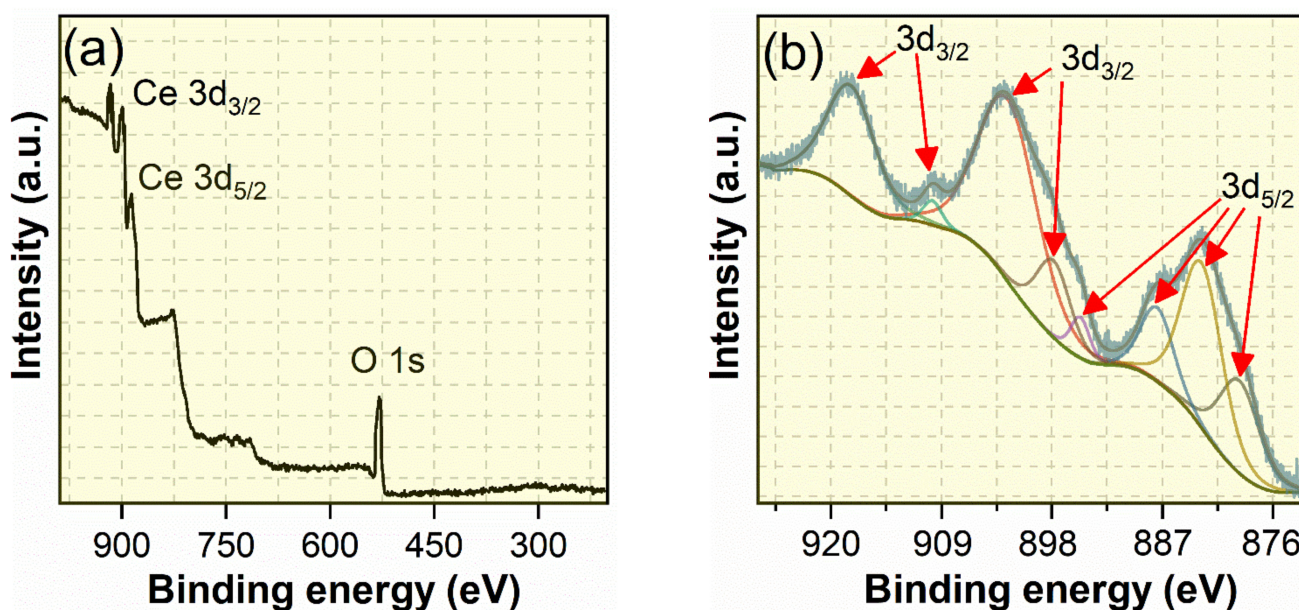


Figure 3. Cont.

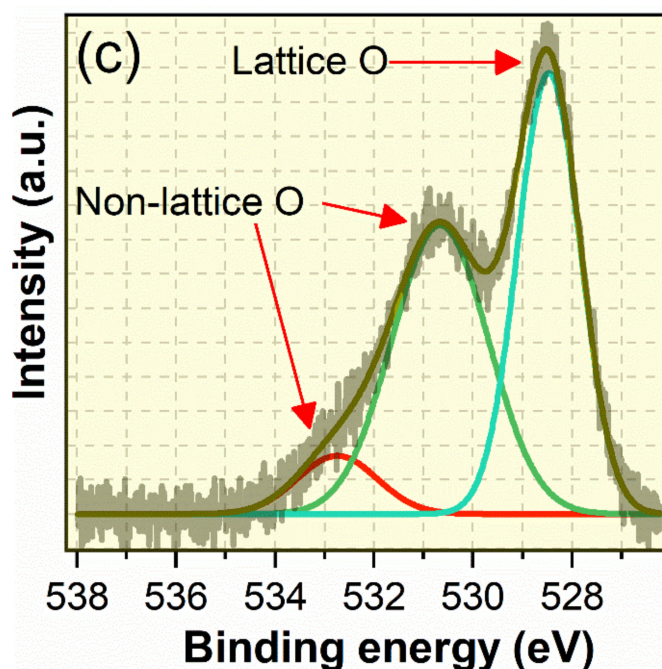


Figure 3. High-resolution XPS spectra of CeO₂: (a) survey scan, (b) Ce 3d, and (c) O 1s.

3.2. Cyclic Voltammetry Analysis

Figure 4a depicts the cyclic voltammograms obtained from various modified glassy GC electrodes under two conditions: in the absence and presence of 0.1 mM Mg²⁺ ions. These experiments were conducted in 0.1 M KCl solution with a pH of 7.0, utilizing a scan rate of 0.01 Vs⁻¹. In the absence of Mg²⁺ ions, the cyclic voltammogram of the unmodified GC electrode displayed no discernible reduction or oxidation peaks. However, upon introducing CeO₂ microcuboids as a modification to the bare GC electrode surface, a well-defined redox peak was prominently observed. The oxidation and reduction peak potentials were measured at 0.207 and 0.124 V, respectively, referenced to the Ag/AgCl electrode. Specifically, the anodic peak potential at 0.207 V (vs. Ag/AgCl) corresponds to the oxidation of Ce³⁺ to Ce⁴⁺, while the cathodic peak potential at 0.124 V (vs. Ag/AgCl) corresponds to the reduction of Ce⁴⁺ to Ce³⁺. To investigate the electrocatalytic effect of CeO₂ microcuboid-modified GC electrode on Mg²⁺ ions, cyclic voltammetry was performed in 0.1 M KCl solution (pH 7.0) containing 0.1 mM Mg²⁺ ions, utilizing a scan rate of 0.01 Vs⁻¹. During the forward scan from -0.13 to 0.72 V, no oxidation peak was observed. However, in the reverse scan, a distinctive cathodic signal arising from the reduction of Mg²⁺ to Mg⁰ was detected at 0.393 V (vs. Ag/AgCl), indicating the irreversibility of the reduction behavior of magnesium ions. To gain a more comprehensive understanding of the electrochemical reduction of Mg²⁺ ions, the number of electrons transferred (*n*) in the electro-reduction process was determined using Equation (2).

$$E_p^c - \frac{E_p^c}{2} = \frac{47.7}{\alpha n} \quad (2)$$

where α is the electron transfer coefficient, E_p^c is the cathodic peak potential and $\frac{E_p^c}{2}$ is the half-peak potential values of Mg²⁺ ion. Given the irreversible nature of the electro-reduction process of Mg²⁺ ions, the value of α was set to 0.5 [29–31]. The calculated number of electrons transferred during the electro-reduction of Mg²⁺ to Mg⁰ was determined to be 2.12 (~2.0). These findings support the conclusion that Mg²⁺ ions acquire two electrons to form Mg⁰. A plausible electro-reduction mechanism for Mg²⁺ ions is illustrated in Figure 1. From Figure 1, it is evident that upon contact of Mg²⁺ ions with the CeO₂ microcuboid-modified GC electrode, the reduction process of Mg²⁺ occurs, leading to the

generation of Mg^0 accompanied by the release of two electrons. This reduction process is facilitated by the electrocatalytic effect of CeO_2 microcuboids on the reduction of Mg^{2+} ions. The electrocatalytic behavior arises from the reversible transformation between the Ce^{3+} and Ce^{4+} oxidation states within the CeO_2 microcuboid-modified GC electrode. This phenomenon significantly promotes the reduction of Mg^{2+} ions, as manifested by the distinct cathodic signal observed during cyclic voltammetry experiments. Subsequently, the two released electrons during the electrocatalytic process are efficiently transferred to the GC electrode through the CeO_2 microcuboids, leading to an enhanced negative current response at the reduction potential of 0.393 V (vs. Ag/AgCl).

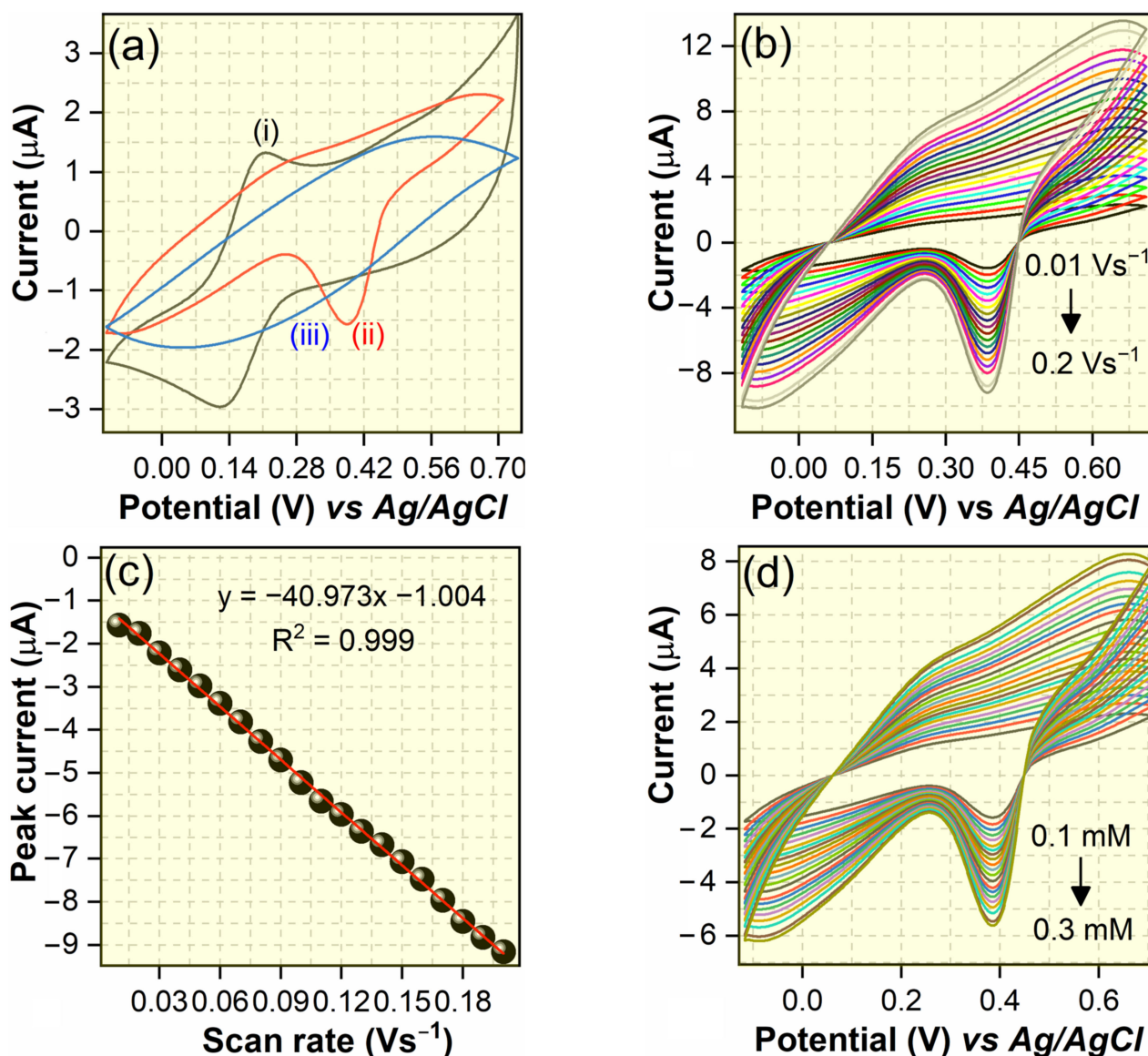


Figure 4. Cont.

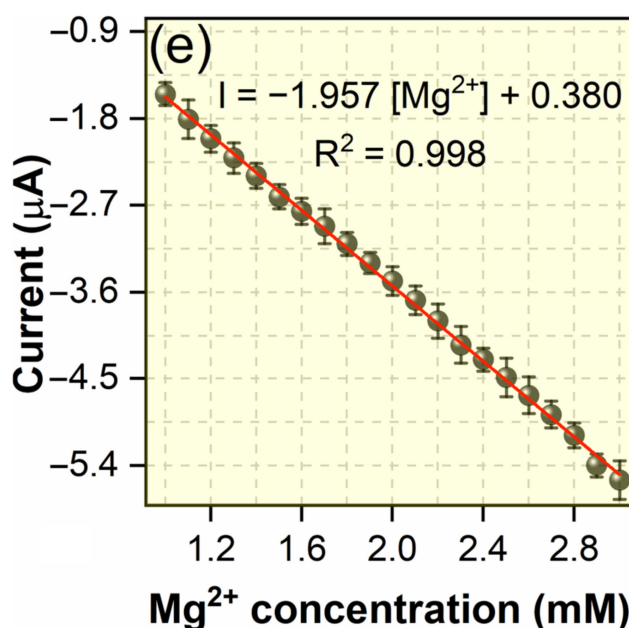


Figure 4. (a) Cyclic voltammograms obtained from various modified electrodes, namely, (i) GC/CeO₂ in the absence of 0.1 mM Mg²⁺ ions, (ii) GC/CeO₂ in the presence of 0.1 mM Mg²⁺ ions, and (iii) bare GCE in the absence of 0.1 mM Mg²⁺ ions. These measurements were conducted in 0.1 M KCl solution (pH 7.0) with a scan rate of 0.01 Vs⁻¹. (b) The effect of scan rate on the cyclic voltammetric responses of GC/CeO₂ electrode for the detection of 0.1 mM Mg²⁺ ions in 0.1 M KCl solution (pH 7.0), (c) the dependence of anodic peak current for Mg²⁺ ions on scan rates, (d) cyclic voltammetric responses of GC/CeO₂ electrode with increasing concentration of Mg²⁺ ions in 0.1 M KCl solution (pH 7.0) at a scan rate of 0.01 Vs⁻¹, and (e) calibration plot of different concentrations of Mg²⁺ ions corresponding to cyclic voltammetry at scan rate of 0.01 Vs⁻¹.

A significant increase in current response of $-1.57 \mu\text{A}$ observed at 0.393 V (vs. Ag/AgCl) was attributed to the enhanced electron transfer rate ($k_s = I_p/Q = 8.94 \text{ s}^{-1}$, where I_p is the peak current and Q is the amount of charge consumed) and high surface coverage of the adsorbed Mg²⁺ ion ($\Gamma = Q/nFA = 2.17 \times 10^{-7} \text{ mol cm}^{-2}$, n is the number of electrons transferred, F is the Faraday constant, and A is the area of electrode) [32,33]. Due to the microcuboid-like structure of CeO₂ microparticles, electron transfer between adsorbed magnesium ions and GCE was facilitated. Taken together, the cyclic voltammetry results compellingly demonstrate the exceptional electrocatalytic effect of CeO₂ microcuboid-modified GC electrode with respect to the irreversible reduction signal of Mg(II).

The effect of scan rate on the cyclic voltammetric response of GC/CeO₂ electrode for the detection of 0.1 mM Mg²⁺ ions in 0.1 M KCl solution (pH 7.0) was studied in the range of 0.01–0.2 Vs⁻¹ (Figure 4b). As shown in Figure 4b, the cathodic peak current of Mg²⁺ reduction increased linearly with the increasing scan rate over the range of 0.01–0.2 Vs⁻¹, indicating a linear relationship between the cathodic peak current and scan rate. This linear relationship is mathematically described by the linear regression equation: $I_p = -40.973[v] - 1.004$, which is accompanied by a highly favorable regression coefficient of 0.999, providing strong evidence of the dependence of the cathodic peak current on the scan rate (Figure 4c). These voltammetric scan rate investigations revealed that the electrochemical reaction of Mg²⁺ ions on the CeO₂ microcuboids/GC electrode adheres to a typical surface-controlled process.

The cyclic voltammetric responses of the GC/CeO₂ electrode were investigated in 0.1 M KCl solution (pH 7.0), employing increasing concentrations of Mg²⁺ ions, at a scan rate of 0.01 Vs⁻¹. The resultant outcomes are depicted in Figure 4d. It is noteworthy that a noticeable increase in the cathodic peak current, associated with the reduction of Mg²⁺, was

observed as the concentration of magnesium ions increased. To establish the relationship between the cathodic peak current and the concentration of Mg^{2+} ions, a calibration plot was constructed based on cyclic voltammetry at a scan rate of 0.01 Vs^{-1} , as depicted in Figure 4e. Remarkably, the cathodic peak current exhibited a linear relationship ($I = -1.957 [\text{Mg}^{2+}] + 0.380$) with the increasing concentration of Mg^{2+} ion within the range of 0.1–0.3 mM. The obtained linear regression analysis yielded a sensitivity of $1.957 \mu\text{A mM}^{-1}$ and a regression coefficient of 0.998, indicating a strong association between the cathodic peak current and the concentration of Mg^{2+} ions. To ascertain the limits of detection (LOD) and quantification (LOQ), the formulas Equation (3) and Equation (4), respectively, were utilized.

$$\text{LOD} = \frac{3 \times \text{Standard deviation of the blank response}}{\text{Slope of the calibration curve}} \quad (3)$$

$$\text{LOQ} = \frac{10 \times \text{Standard deviation of the blank response}}{\text{Slope of the calibration curve}} \quad (4)$$

The calculated values for LOD and LOQ are 30 and 100 μM , respectively.

3.3. Differential Pulse Voltammetric Detection of $\text{Mg}(\text{II})$ Ions Using CeO_2 Microcuboids/GCE

Figure 5a presents the differential pulse voltammetric profiles obtained from various concentrations (0.1–3 mM) of Mg^{2+} ions in 0.1 M KCl solution at pH 7.0. It is noteworthy that an increase in the cathodic peak current, exhibiting a negative trend, is observed as the concentration of Mg^{2+} ion rises. Furthermore, a strong linear correlation is evident between the cathodic current and the Mg^{2+} ion concentrations, as demonstrated by a linear regression equation of $I = -2.357 [\text{Mg}^{2+}] + 0.321$ and a regression coefficient of 0.996 (Figure 5b). The developed electrode exhibits a remarkable sensitivity of $2.357 \mu\text{A mM}^{-1}$, encompassing a broad linear detection range of 0.1–3 mM. The detection and quantification limits are impressively low, with values of 22.35 and 74.42 μM , respectively.

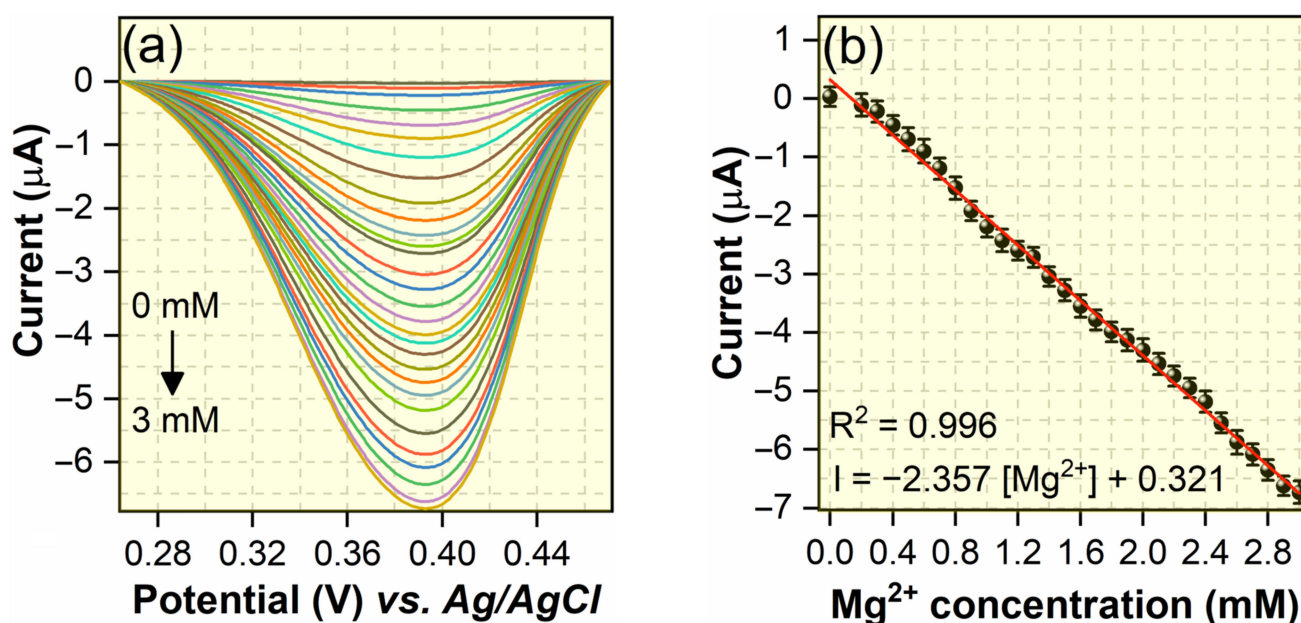


Figure 5. Cont.

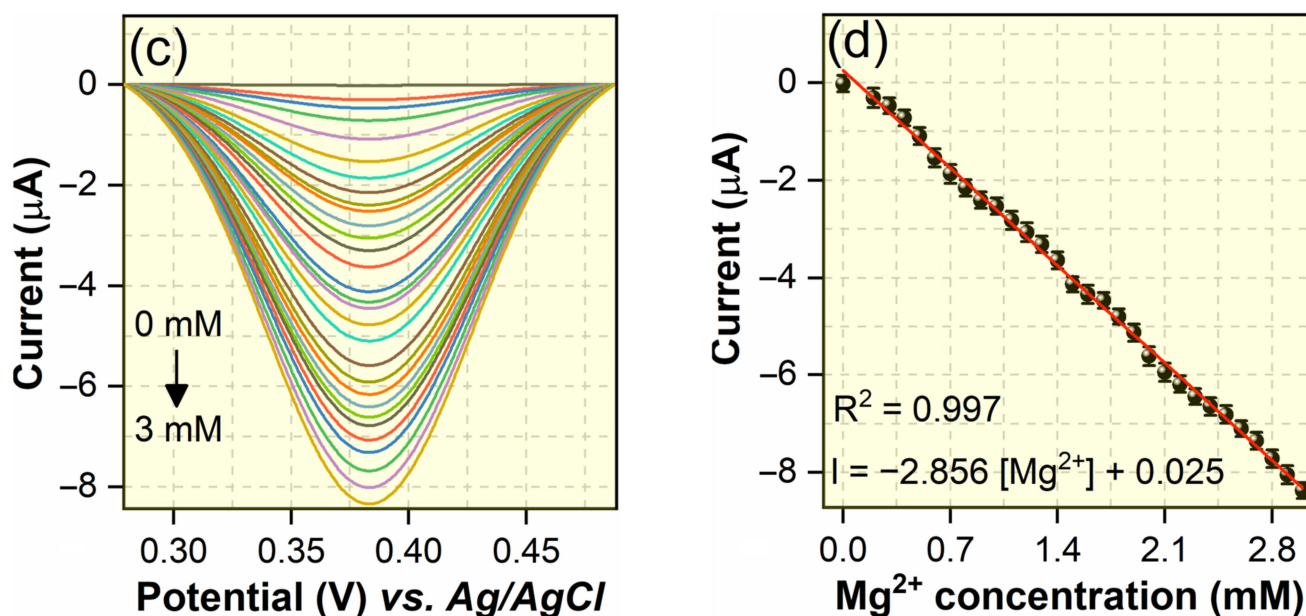


Figure 5. (a) Differential pulse voltammetric curves of different concentrations of Mg^{2+} ions (0.1–3 mM) in 0.1 M KCl solution (pH 7.0) and its (b) calibration curve for Mg^{2+} ions. (c) Square wave voltammograms of various concentrations of Mg^{2+} ions (0.1–3 mM) measured with GC/ CeO_2 and (d) calibration curve achieved from square wave voltammetric measurements for different concentrations of Mg^{2+} ions in 0.1 M KCl solution (pH 7.0).

3.4. Square Wave Voltammetric Detection of Mg(II) Ions Using CeO_2 Microcuboids/GCE

Since electrochemical analysis based on square wave voltammetry is more sensitive than analysis based on differential pulse voltammetry for the detection of an analyte of interest, electrochemical analysis of Mg^{2+} ions in the same microenvironment was carried out employing the square wave voltammetry technique with CeO_2 microcuboid-modified GCE as the working electrode [34,35]. Figure 5c shows the square wave voltammograms of various concentrations of Mg^{2+} ions (0.1–3 mM) measured with GC/ CeO_2 . Similarly to the differential pulse voltammetry profile, the square wave voltammetry profile exhibits a discernible negative trend with increasing concentrations of Mg^{2+} ions. Figure 5c illustrates a robust linear relationship ($I = -2.856 [\text{Mg}^{2+}] + 0.025$, $R^2 = 0.997$) between the cathodic peak current and the concentration of Mg^{2+} ions. Furthermore, the reduction peak current of Mg^{2+} ions demonstrates a direct proportionality to their concentration within the examined range of 0.1–3 mM. The developed electrode displayed a high sensitivity of $2.856 \mu\text{A mM}^{-1}$, along with a notably low detection limit of $19.84 \mu\text{M}$, and quantification limit of $66.06 \mu\text{M}$, respectively. A comprehensive analysis of the analytical performance attributes of the Mg^{2+} sensor utilizing square wave voltammetry versus those utilizing cyclic voltammetry and differential pulse voltammetry reveals that only the square wave voltammetry-based Mg^{2+} sensor possesses superior characteristics. Specifically, the square wave voltammetry-based Mg^{2+} sensor exhibits a lower detection limit, a lower quantification limit, and increased sensitivity, proving its superiority over cyclic voltammetry and differential pulse voltammetry-based Mg^{2+} sensors.

In order to predict the level of magnesium ions and establish a quantitative relationship between magnesium ion levels and electrochemical parameters, various electrochemical characteristics were assessed from square wave voltammograms. These characteristics include the area beneath the peak current, the cathodic peak current, the highest ascending slope, and the lowest descending slope (Figure 6a–d). By considering different concentrations of magnesium ions, multiple linear regression and partial least squares regression models were developed using the estimated electrochemical parameters. The fitted multi-

ple linear regression (Equation (5)) and partial least squares regression models (Equation (6)) are as follows:

$$[Mg^{2+}] = 0.098 + 2.330 \times 10^{10} [peak\ area] - 3.176 \times 10^{11} [\Gamma] + 5.908 [maximum\ slope] - 5.856 [minimum\ slope] - 2096.925 [I_p] \quad (5)$$

$$[Mg^{2+}] = 0.102 + 6.300 [peak\ area] + 85.898 [\Gamma] + 4.381 [maximum\ slope] - 4.865 [minimum\ slope] - 1276.586 [I_p] \quad (6)$$

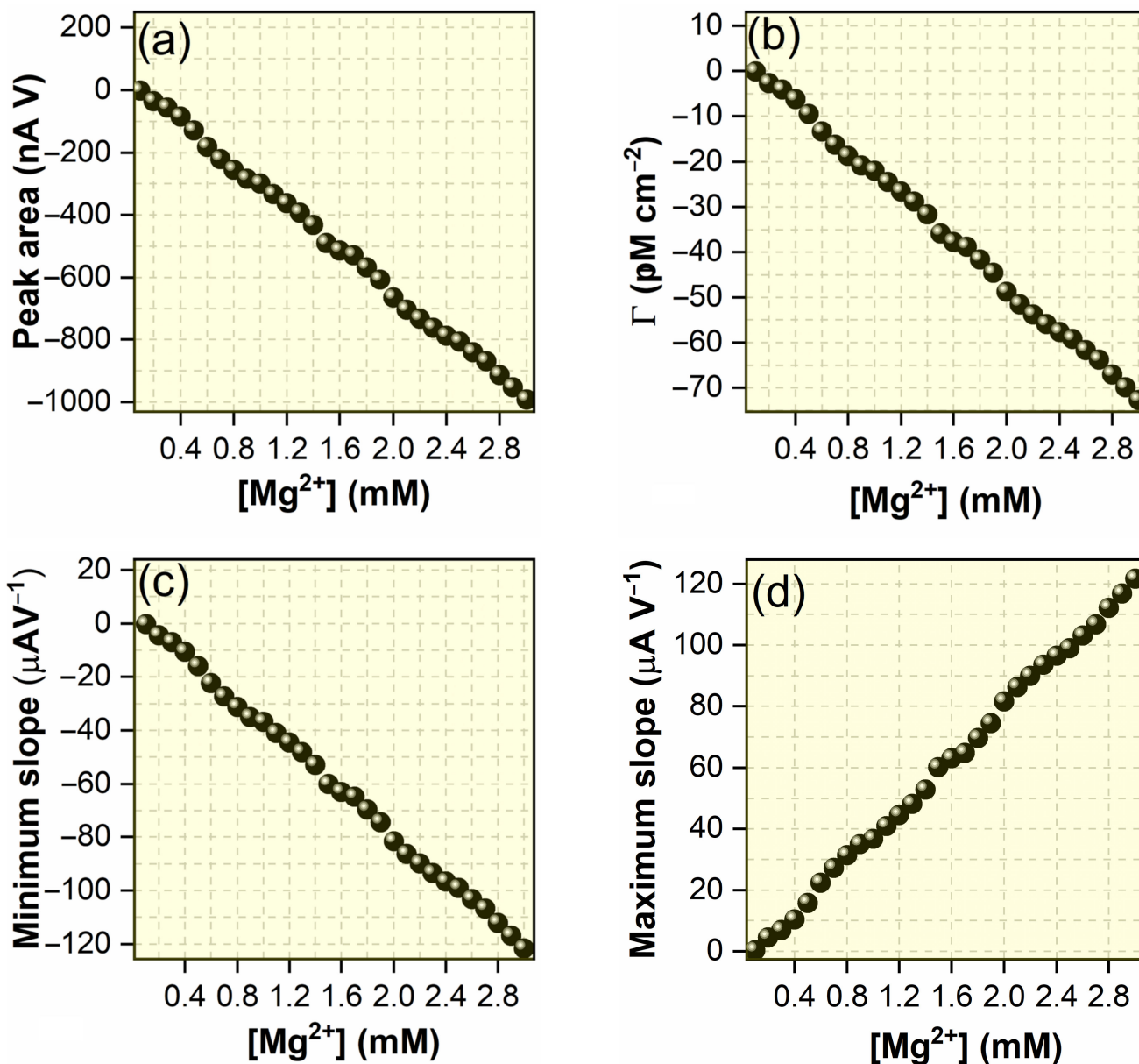


Figure 6. (a) Plot of peak area versus the concentration of Mg^{2+} , (b) plot of surface coverage versus the concentration of Mg^{2+} , (c) plot of minimum slope estimated from square wave voltammograms versus the concentration of Mg^{2+} , and (d) plot of maximum slope estimated from square wave voltammograms versus the concentration of Mg^{2+} .

The predictive performance of the models for determining magnesium ion concentration in 0.1 M KCl (pH 7.0) was evaluated using the relative prediction error (RPE). The RPE values for the fitted partial least squares regression and multiple linear regression models were determined to be 0.078% and 0.075%, respectively. This indicates that the proposed multiple linear regression model exhibits greater accuracy in predicting magnesium ion levels in 0.1 M KCl (pH 7.0) compared to the proposed partial least squares regression model.

3.5. Amperometric Detection of Mg(II) Ions at CeO₂ Microcuboids/GCE

The amperometric current responses to incremental concentrations of Mg²⁺ ions (ranging from 0 to 3 mM) in 0.1 M KCl solution at pH 7.0 were examined at an applied potential of 0.393 V (vs Ag/AgCl), as shown in Figure 7. With an increasing concentration of magnesium ions, a corresponding elevation in the amperometric current was observed. Figure 7b shows the calibration curve of the amperometric current response to Mg²⁺ ion concentrations, ranging from 0 to 3 mM. The plot of amperometric current against the concentration of Mg²⁺ ions demonstrates a linear relationship, characterized by a well-defined straight line, thereby affirming the linear dependence of the amperometric current on the concentration of Mg²⁺ ions. The associated linear regression equation is expressed as $I = -2.382 [\text{Mg}^{2+}] + 0.044$, and the R² attains a value of 0.998, indicating a high level of correlation. Moreover, the fabricated CeO₂ microcuboids/GCE exhibits a remarkable level of sensitivity (2.382 $\mu\text{A mM}^{-1}$) over a wide linear range spanning from 0 to 3 mM, accompanied by a low detection limit of 19.92 μM and a quantification limit of 66.33 μM . The superior performance of the fabricated electrode can be attributed to the synergistic effects resulting from the enhanced electrocatalytic activity of CeO₂ microcuboids towards magnesium ions, the increased electron transfer rate, and the enhanced adsorption capacity of magnesium ions on the CeO₂ microcuboids/GCE surface. Notably, the developed electrode showcases a rapid response time of less than 140 s.

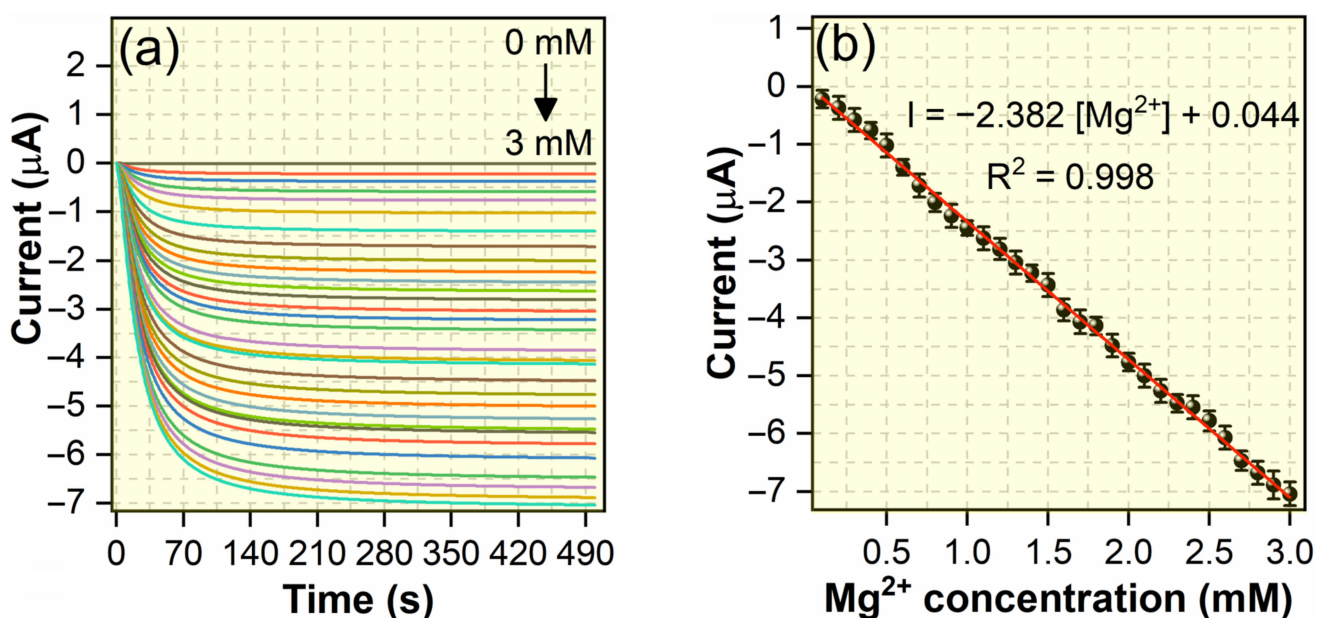


Figure 7. Cont.

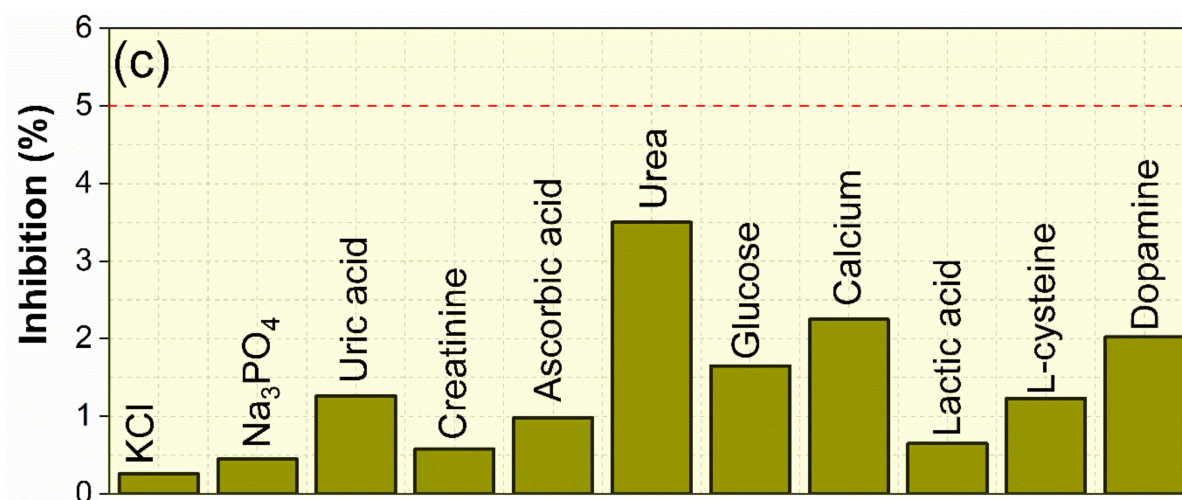


Figure 7. (a) Amperometric current responses for the increasing concentrations of Mg^{2+} ions (0–3 mM) in 0.1 M KCl solution (pH 7.0) at 0.393 V (vs. Ag/AgCl), (b) calibration curve of the amperometric current response to the concentration of Mg^{2+} ions ranging from 0 to 3 mM, and (c) plot of percentage inhibition of the CeO_2 -modified GCE against the different potential interfering species.

3.6. Repeatability, Reproducibility, Interferences, and Stability Studies

In order to evaluate the repeatability of the CeO_2 microcuboid-modified GCE, twelve consecutive measurements were carried out in 0.1 M KCl solution (pH 7.0) containing 0.1 mM Mg^{2+} ions. Throughout the twelve runs, a marginal decline in the square wave voltammetric current response was observed, accompanied by a relative standard deviation (RSD) of 1.62%. These findings indicate the excellent repeatability of the fabricated electrode. In order to assess the reproducibility of the developed Mg^{2+} ion sensor, twelve parallel electrodes were developed and tested independently in 0.1 M KCl solution (pH 7.0) containing 0.1 mM Mg^{2+} ions. The corresponding square wave voltammetric current responses were recorded, yielding an RSD of 2.68%. This outcome signifies that the fabricated sensor exhibits satisfactory reproducibility. The selectivity of the CeO_2 microcuboid-modified GCE towards magnesium ions was investigated by measuring the square wave voltammetric current response of 0.1 mM of magnesium ions in the presence of potentially interfering species, including potassium chloride, trisodium phosphate, uric acid, creatinine, L-cysteine, lactic acid, calcium ions, dopamine, glucose, urea, and ascorbic acid, each at a concentration of 1 mM. A tenfold excess of these potentially interfering species was added to 0.1 M KCl solution (pH 7.0) containing 0.1 mM Mg^{2+} ion and the resulting square wave voltammograms were recorded to calculate the percentage inhibition. Figure 7c shows the plot of percentage inhibition of the CeO_2 -modified GCE against the different potential interfering species. A tolerance limit of less than 5% was established, as exceeding this threshold indicates the ability of potential interfering species to impede the sensor's accurate detection and quantification of magnesium ions in 0.1 M KCl solution. The tested potentially interfering species did not exhibit a discernible difference in the percentage of inhibition, with the exception of uric acid, which significantly affected the inhibition percentage. These results imply that the interference caused by the tested molecules is negligible, underscoring the high selectivity of the developed electrode for Mg^{2+} ions. In addition, the operational stability of the developed electrode was studied by measuring the square wave voltammetric current response for 0.1 mM Mg^{2+} ion every 2 days. The experimental study revealed a decrease in the square wave voltammetric current response from 98% to 96.57% of its initial value after 10 and 20 days, respectively, indicating that the CeO_2 microcuboid-modified GCE has significant potential for electrochemical detection of $Mg(II)$ ions.

Table 1 presents a comparative analysis of the performance of the proposed sensing platform with previously reported electrochemical sensors designed specifically for the detection of Mg^{2+} ions. Among the various sensors investigated, it is noteworthy that only the

CeO₂ microcuboid-modified GCE demonstrated a detection limit lower than those reported in the existing literature. Importantly, the conventional approach adopted by the previous studies involved establishing a calibration equation based solely on linear regression for Mg²⁺ ion sensing. In contrast, this study employed a more comprehensive approach by utilizing linear regression, multiple linear regression, and partial least squares regression techniques to develop robust calibration equations for the electrochemical determination of Mg²⁺ ions in 0.1 M KCl.

Table 1. Comparison of the performance of the proposed sensing platform with other reported electrochemical sensors designed for the detection of Mg²⁺ ions.

Material	Linearity (mM)	LOD (μM)	Regression	Adjusted R ²	References
MWCNTs/polydimethylsiloxane/graphite	0.041–8.228	---	Linear	0.99	[5]
Mg ²⁺ -dependent DNAzyme/Au	0.2–5.0	50	Linear	0.99	[6]
ZnO nanorods/Ag	5 × 10 ⁻⁴ –100	---	Linear	0.99	[7]
Ionophore/PVC/NaTPB/DOP/glass	0.01–100	---	Linear	---	[8]
Chlorophyll/PVC	0.01–100	---	Linear	---	[9]
CeO ₂ /GC	0–3	19.84	Linear, multiple linear, partial least squares	0.99	This work

4. Conclusions

In this study, we employed CeO₂ microcuboids GCE for the purpose of ultrasensitive and selective detection of Mg(II) ions. The synthesis of CeO₂ microparticles was accomplished using microwave radiation, resulting in the formation of micro-cuboid structures of 167 nm in width, 163 nm in height, and 976 nm in length. It is worth noting that the CV results exhibited a remarkable electrocatalytic effect of the CeO₂ microcuboid-modified GC electrode, particularly in relation to the irreversible reduction signal of Mg(II). Comparatively, when assessing the electrochemical performance of various Mg(II) ion sensors based on cyclic voltammetry, amperometry, and differential pulse voltammetry techniques, only the square wave voltammetry approach yielded superior sensitivity (2.856 μA mM⁻¹) across a wide linear range spanning from 0 to 3 mM. Additionally, the square wave voltammetry-based sensor exhibited a lower detection limit of 19.84 μM and a quantification limit of 66.06 μM. Notably, the developed electrode showcases a rapid response time of less than 140 s. These findings emphasize the superior performance achieved through the utilization of CeO₂ microcuboids, which offered enhanced electrocatalytic activity towards magnesium ions, increased electron transfer rate, and enhanced adsorption capacity of magnesium ions on the CeO₂ microcuboids/GCE surface. Both multiple linear regression and partial least squares regression models were developed to establish a quantitative relationship between magnesium ion levels and electrochemical parameters. In summary, the multi-electrochemical parameter-dependent calibration equation, low detection limit, rapid response time, good stability, excellent reproducibility, enhanced Mg(II) adsorption, high electron transfer rate, and anti-interference ability are the array of advantageous characteristics of the CeO₂ microcuboid-modified GCE that make them popular for Mg(II) sensing.

Author Contributions: G.M.: conceptualization, design, supervision, writing—original draft, editing. N.N.: experiments, design, analysis, writing—original draft, editing. A.J.K.: design, writing. J.B.B.R.: conceptualization, supervision, writing—review and editing. B.M.G.: design, analysis. All authors have read and agreed to the published version of the manuscript.

Funding: This research was funded by the Department of Science and Technology, New Delhi, grant SR/FST/ET-I/2018/221(c) and Professor T.R. Rajagopalan Research Fund, SASTRA Deemed University.

Institutional Review Board Statement: Not applicable.

Informed Consent Statement: Not applicable.

Data Availability Statement: Not applicable.

Acknowledgments: We acknowledge SASTRA Deemed University, Thanjavur for extending infrastructure support to carry out the study.

Conflicts of Interest: The authors declare no conflict of interest.

References

1. Gonzalez, J.; Hou, R.Q.; Nidadavolu, E.P.S.; Willumeit-Römer, R.; Feyereabend, F. Magnesium Degradation under Physiological Conditions—Best Practice. *Bioact. Mater.* **2018**, *3*, 174–185. [[CrossRef](#)]
2. Glasdam, S.-M.; Glasdam, S.; Peters, G.H. *Chapter Six—The Importance of Magnesium in the Human Body: A Systematic Literature Review*; Elsevier: Amsterdam, The Netherlands, 2016; Volume 73, pp. 169–193. ISBN 0065-2423.
3. De Baaij, J.H.F.; Hoenderop, J.G.J.; Bindels, R.J.M. Magnesium in Man: Implications for Health and Disease. *Physiol. Rev.* **2015**, *95*, 1–46. [[CrossRef](#)]
4. Topf, J.M.; Murray, P.T. Hypomagnesemia and Hypermagnesemia. *Rev. Endocr. Metab. Disord.* **2003**, *4*, 195–206. [[CrossRef](#)] [[PubMed](#)]
5. Akhter, F.; Nag, A.; Alahi, M.E.E.; Liu, H.; Mukhopadhyay, S.C. Electrochemical Detection of Calcium and Magnesium in Water Bodies. *Sens. Actuators A Phys.* **2020**, *305*, 111949. [[CrossRef](#)]
6. Gao, X.; Huang, H.; Niu, S.; Ye, H.; Lin, Z.; Qiu, B.; Chen, G. Determination of Magnesium Ion in Serum Samples by a DNAzyme-Based Electrochemical Biosensor. *Anal. Methods* **2012**, *4*, 947–952. [[CrossRef](#)]
7. Asif, M.H.; Ali, S.M.U.; Nur, O.; Willander, M.; Englund, U.H.; Elinder, F. Functionalized ZnO Nanorod-Based Selective Magnesium Ion Sensor for Intracellular Measurements. *Biosens. Bioelectron.* **2010**, *26*, 1118–1123. [[CrossRef](#)] [[PubMed](#)]
8. Gupta, V.K.; Chandra, S.; Mangla, R. Magnesium-Selective Electrodes. *Sens. Actuators B Chem.* **2002**, *86*, 235–241. [[CrossRef](#)]
9. Lü, H.; Zhao, Y.; Ma, J.; Li, J.; Wang, H.; Lu, Z. Electrochemical Detection of Magnesium Ions Using PVC Membrane Trapped Chlorophyll A Molecules. *Mol. Cryst. Liq. Cryst. Sci. Technol. Sect. A Mol. Cryst. Liq. Cryst.* **2001**, *371*, 391–396. [[CrossRef](#)]
10. Kim, D.-Y.; Shinde, S.; Ghodake, G. Colorimetric Detection of Magnesium (II) Ions Using Tryptophan Functionalized Gold Nanoparticles. *Sci. Rep.* **2017**, *7*, 3966. [[CrossRef](#)]
11. Karimi-Maleh, H.; Karimi, F.; Alizadeh, M.; Sanati, A.L. Electrochemical Sensors, a Bright Future in the Fabrication of Portable Kits in Analytical Systems. *Chem. Rec.* **2020**, *20*, 682–692. [[CrossRef](#)]
12. Xue, S.; Li, Q.; Wang, L.; You, W.; Zhang, J.; Che, R. Copper- and Cobalt-Codoped CeO₂ Nanospheres with Abundant Oxygen Vacancies as Highly Efficient Electrocatalysts for Dual-Mode Electrochemical Sensing of MicroRNA. *Anal. Chem.* **2019**, *91*, 2659–2666. [[CrossRef](#)] [[PubMed](#)]
13. Gowthaman, N.S.K.; Ngee Lim, H.; Balakumar, V.; Shankar, S. Ultrasonic Synthesis of CeO₂@organic Dye Nanohybrid: Environmentally Benign Rapid Electrochemical Sensing Platform for Carcinogenic Pollutant in Water Samples. *Ultrason. Sonochem.* **2020**, *61*, 104828. [[CrossRef](#)] [[PubMed](#)]
14. Ansari, S.; Ansari, M.S.; Dev, N.; Satsangee, S.P. CeO₂ Nanoparticles Based Electrochemical Sensor for an Anti-Anginal Drug. *Mater. Today Proc.* **2019**, *18*, 1210–1219. [[CrossRef](#)]
15. Yang, S.; Li, G.; Wang, G.; Liu, L.; Wang, D.; Qu, L. Synthesis of Highly Dispersed CeO₂ Nanoparticles on N-Doped Reduced Oxide Graphene and Their Electrocatalytic Activity toward H₂O₂. *J. Alloys Compd.* **2016**, *688*, 910–916. [[CrossRef](#)]
16. Abdelrahim, M.Y.M.; Benjamin, S.R.; Cubillana-Aguilera, L.M.; Naranjo-Rodríguez, I.; De Cisneros, J.L.H.-H.; Delgado, J.J.; Palacios-Santander, J.M. Study of the Electrocatalytic Activity of Cerium Oxide and Gold-Studded Cerium Oxide Nanoparticles Using a Sonogel-Carbon Material as Supporting Electrode: Electroanalytical Study in Apple Juice for Babies. *Sensors* **2013**, *13*, 4979–5007. [[CrossRef](#)]
17. Hirst, S.M.; Karakoti, A.S.; Tyler, R.D.; Sriranganathan, N.; Seal, S.; Reilly, C.M. Anti-Inflammatory Properties of Cerium Oxide Nanoparticles. *Small* **2009**, *5*, 2848–2856. [[CrossRef](#)]
18. Dhall, A.; Self, W. Cerium Oxide Nanoparticles: A Brief Review of Their Synthesis Methods and Biomedical Applications. *Antioxidants* **2018**, *7*, 97. [[CrossRef](#)]
19. Dunnick, K.M.; Pillai, R.; Pisane, K.L.; Stefaniak, A.B.; Sabolsky, E.M.; Leonard, S.S. The Effect of Cerium Oxide Nanoparticle Valence State on Reactive Oxygen Species and Toxicity. *Biol. Trace Elem. Res.* **2015**, *166*, 96–107. [[CrossRef](#)]
20. Nesakumar, N.; Sethuraman, S.; Krishnan, U.; Rayappan, J.B.B. Electron Transfer Properties of Nano-Ceria Based Linear Voltammetric Biosensor for Tributyrin Detection. *J. Comput. Theor. Nanosci.* **2015**, *12*, 944–949. [[CrossRef](#)]
21. Sayyed, S.A.A.R.; Beedri, N.I.; Kadam, V.S.; Pathan, H.M. Rose Bengal-Sensitized Nanocrystalline Ceria Photoanode for Dye-Sensitized Solar Cell Application. *Bull. Mater. Sci.* **2016**, *39*, 1381–1387. [[CrossRef](#)]
22. Farahmandjou, M.; Zarinkamar, M.; Firoozabadi, T. Synthesis of Cerium Oxide (CeO₂) Nanoparticles Using Simple CO-Precipitation Method. *Rev. Mex. Fis.* **2016**, *62*, 496–499.
23. Culica, M.E.; Chibac-Scutaru, A.L.; Melinte, V.; Coseri, S. Cellulose Acetate Incorporating Organically Functionalized CeO₂ NPs: Efficient Materials for UV Filtering Applications. *Materials* **2020**, *13*, 2955. [[CrossRef](#)] [[PubMed](#)]

24. Chelliah, M.; Rayappan, J.B.B.; Krishnan, U. Synthesis and Characterization of Cerium Oxide Nanoparticles by Hydroxide Mediated Approach. *J. Appl. Sci.* **2012**, *12*, 1734–1737. [[CrossRef](#)]
25. Zamiri, R.; Abbastabar Ahangar, H.; Kaushal, A.; Zakaria, A.; Zamiri, G.; Tobaldi, D.; Ferreira, J.M.F. Dielectrical Properties of CeO₂ Nanoparticles at Different Temperatures. *PLoS ONE* **2015**, *10*, e0122989.
26. Bortamuly, R.; Konwar, G.; Boruah, P.K.; Das, M.R.; Mahanta, D.; Saikia, P. CeO₂-PANI-HCl and CeO₂-PANI-PTSA Composites: Synthesis, Characterization, and Utilization as Supercapacitor Electrode Materials. *Ionics* **2020**, *26*, 5747–5756. [[CrossRef](#)]
27. Lian, J.; Liu, P.; Jin, C.; Shi, Z.; Luo, X.; Liu, Q. Perylene Diimide-Functionalized CeO₂ Nanocomposite as a Peroxidase Mimic for Colorimetric Determination of Hydrogen Peroxide and Glutathione. *Microchim. Acta* **2019**, *186*, 332. [[CrossRef](#)]
28. Channei, D.; Inceesungvorn, B.; Wetchakun, N.; Ukritnukun, S.; Nattestad, A.; Chen, J.; Phanichphant, S. Photocatalytic Degradation of Methyl Orange by CeO₂ and Fe-Doped CeO₂ Films under Visible Light Irradiation. *Sci. Rep.* **2014**, *4*, 5757. [[CrossRef](#)]
29. Guidelli, R.; Compton, R.G.; Feliu, J.M.; Gileadi, E.; Lipkowski, J.; Schmickler, W.; Trasatti, S. Defining the Transfer Coefficient in Electrochemistry: An Assessment (IUPAC Technical Report). *Pure Appl. Chem.* **2014**, *86*, 245–258. [[CrossRef](#)]
30. Houcini, H.; Laghrib, F.; Bakasse, M.; Lahrich, S.; El Mhammedi, M.A. Catalytic Activity of Gold for the Electrochemical Reduction of P-Nitrophenol: Analytical Application. *Int. J. Environ. Anal. Chem.* **2020**, *100*, 1566–1577. [[CrossRef](#)]
31. Li, X.; Drews, T.O.; Rusli, E.; Xue, F.; He, Y.; Braatz, R.; Alkire, R. Effect of Additives on Shape Evolution during Electrodeposition: I. Multiscale Simulation with Dynamically Coupled Kinetic Monte Carlo and Moving-Boundary Finite-Volume Codes. *J. Electrochem. Soc.* **2007**, *154*, D230. [[CrossRef](#)]
32. Nesakumar, N.; Anantharaj, S.; Subramanian, N.; Kundu, S.; Alwarappan, S. NiFe-Layered Double Hydroxide Sheets as an Efficient Electrochemical Biosensing Platform. *J. Electrochem. Soc.* **2018**, *165*, B536–B542. [[CrossRef](#)]
33. Nesakumar, N.; Ramachandra, B.L.; Sethuraman, S.; Krishnan, U.M.; Rayappan, J.B.B. Theoretical Investigation of Surface Coverage in the Electrochemical Behaviour of Enzyme Modified Electrodes. *Sens. Lett.* **2015**, *13*, 344–348. [[CrossRef](#)]
34. Elqudaby, H.M.; Mohamed, G.G.; El Din, G.M.G. Electrochemical Behaviour of Trimebutine at Activated Glassy Carbon Electrode and Its Direct Determination in Urine and Pharmaceuticals by Square Wave and Differential Pulse Voltammetry. *Int. J. Electrochem. Sci.* **2014**, *9*, 856–869. [[CrossRef](#)]
35. Uslu, B.; Özkan, S.A.; Şentürk, Z. Electrooxidation of the Antiviral Drug Valacyclovir and Its Square-Wave and Differential Pulse Voltammetric Determination in Pharmaceuticals and Human Biological Fluids. *Anal. Chim. Acta* **2006**, *555*, 341–347. [[CrossRef](#)]

Disclaimer/Publisher’s Note: The statements, opinions and data contained in all publications are solely those of the individual author(s) and contributor(s) and not of MDPI and/or the editor(s). MDPI and/or the editor(s) disclaim responsibility for any injury to people or property resulting from any ideas, methods, instructions or products referred to in the content.